Functionalized Graphene Sheet Colloids for Enhanced Fuel/Propellant Combustion

Justin L. Sabourin,[†] Daniel M. Dabbs,[‡] Richard A. Yetter,[†,*] Frederick L. Dryer,[§] and Ilhan A. Aksay[‡,*]

[†]Department of Mechanical and Nuclear Engineering, The Pennsylvania State University, University Park, Pennsylvania 16802, and [‡]Department of Chemical Engineering and [§]Department of Mechanical and Aerospace Engineering, Princeton University, Princeton, New Jersey 08544

T he success of many future high speed propulsion systems will depend on the ability to use environmentally friendly liquid fuels that offer high energy density, high heat sink capacity, short ignition delays, high reaction rates, and low cost (*i.e.*, are easy to handle and readily available).[1,2] One of the problems with new and/or alternative fuels is that they often perform less satisfactorily than fuels currently in use.[3,4] Recently there has been considerable interest in using colloidal suspensions consisting of low concentrations of colloids dispersed within a liquid hydrocarbon fuel to improve ignition and enhance the performance characteristics of the fuel.[5,6] The colloidal particles, which are dispersed within the fuel during storage and handling, can facilitate endothermic fuel characteristics in the fuel delivered to the engine (*i.e.*, as a liquid fuel catalyst) and then can be used to enhance ignition and combustion once the fuel is vaporized and appropriately mixed. During the fuel addition and mixing in the combustion chamber, particles are homogeneously dispersed throughout the gas-phase reaction zone, where they catalyze reactions. Nanostructured additives offer distinct advantages over larger scale particles due to their high surface area to volume ratio and increased density of surface functionalities. Nanoscale materials also exhibit optical properties favorable to radiative heat transfer that could aid in combustion.[7] Colloids containing various nanostructured ignition agents may allow for the distributed ignition (or heating) of fuels using light sources; distributed ignition, as opposed to single-point ignition, could greatly improve combustion efficiencies.[8] These properties allow for greater heating rates of the individual particles, increased numbers of active surface sites, and

enhanced reactivity. Furthermore, the heat sink properties of the liquid may be significantly enhanced by low concentrations of nanoparticle additives in the liquid.[9−12] A colloidal catalyst dispersed in the fuel is particularly appealing because it can be readily integrated into existing and future liquid combustion systems.

Colloidal dispersions are also of interest for solving combustion related issues in other energy conversion devices. For example, colloidal dispersions of nanocatalysts in automotive diesel fuels are receiving attention as a means to improve cetane numbers and fuel economy, as well as to increase soot reactivity in particulate filter traps.[13,14] In addition to hydrocarbon-based fuels for air-breathing propulsion applications, the use of nanocatalysts in monopropellant and bipropellant rocket applications may eliminate the need for more elaborate structural catalysts, thereby enabling the use of expendable catalysts and novel high energy density monopropellants.[15] For hypergolic applications, colloidal catalysts may also permit the substitution of less reactive nontoxic reactants by reducing ignition delays.[16]

ABSTRACT We have compared the combustion of the monopropellant nitromethane with that of nitromethane containing colloidal particles of functionalized graphene sheets or metal hydroxides. The linear steady-state burning rates of the monopropellant and colloidal suspensions were determined at room temperature, under a range of pressures (3.35−14.4 MPa) using argon as a pressurizing fluid. The ignition temperatures were lowered and burning rates increased for the colloidal suspensions compared to those of the liquid monopropellant alone, with the graphene sheet suspension having significantly greater burning rates (*i.e.*, greater than 175%). The relative change in burning rate from neat nitromethane increased with increasing concentrations of fuel additives and decreased with increasing pressure until at high pressures no enhancement was found.

KEYWORDS: graphene · metal oxide · nanoparticle · nitromethane · combustion · propellant
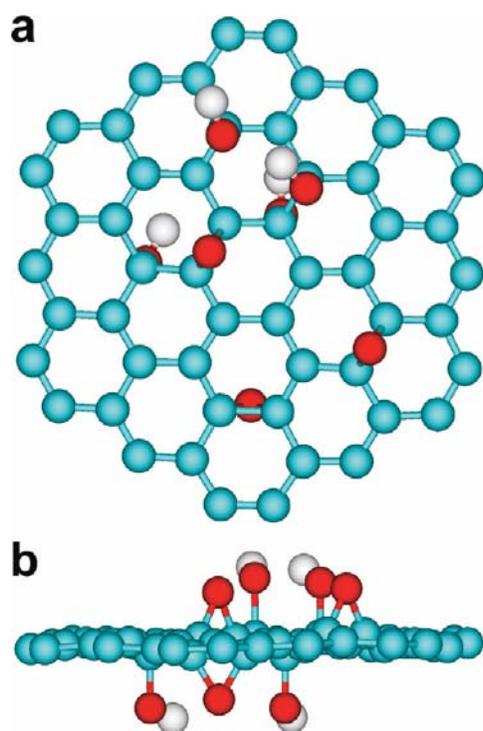
© 2009 American Chemical Society

Figure 1. Functional groups on graphene. (a) A planar view showing epoxides and hydroxides above and below the graphene plane. Carbon atoms are blue, oxygen atoms are red, and hydrogen atoms are white. (b) Edge-on view of a functionalized graphene sheet with distribution of functionalities above and below the plane. The estimated thickness of a functionalized graphene sheet with functionalities is ~0.78 nm.[23]

The majority of work to date involving the use of nanocatalytic and/or energetic fuel additives has involved the use of metals and/or metal oxides or oxyhydroxides. Although these systems have enhanced performance, there are accompanying disadvantages. Nanoscale metal additives, usually aluminum, can significantly increase energy densities and reaction rates of propellants.[17−21] However, performance is compromised by the presence of nonenergetic oxide passivation layers on the particles,[22] and the production of solid oxide reaction products in the combustion process. Many of these problems could be solved by using a support material that not only catalyzes fuel combustion reactions but eventually participates energetically and is consumed without producing residual particulates. Here, we show that functionalized graphene sheets (FGSs)[23,24] (Figure 1) address these issues and represent a new approach for nanostructured fuel additives.

Graphene, the name given to a single basal plane of graphite, is a two-dimensional (2D) honeycomb arrangement of sp^2 bound carbon atoms. These 2D carbon layers are the building blocks for other carbon materials, including carbon nanotubes (CNTs), bulk graphite, and buckyballs.[25] Graphene sheets exhibit many of the same desirable qualities as CNTs, including high electrical conductivity and good mechanical

properties, but should not contain significant quantities of metal particles that are used to catalyze CNT growth as the synthesis of FGS does not use metal-containing catalysts.[23,24,26,27] FGS, as the functionalized form of the graphene sheet, differs from ideal graphene in that it contains chemical functional groups on the surface (epoxides and hydroxides) (Figure 1) and on the edges (hydroxides and carboxylates).[23,24,28] The carbon to oxygen (C/O) ratio can range from 2 ("graphene oxide") to higher values, depending on the degree of reduction.[23,24] The nominal C/O (mol/mol) ratio is designated by a numeric subscript, hence FGS_{22} has a C/O ratio of 22. Chemical or thermal reduction of the FGS increases the C/O ratio by removing carbon oxides, which creates vacancies and topographical defects in the FGS.[23,29] These surface defects cause the FGS to buckle, fold, and wrinkle, helping to prevent regraphitization of the FGSs by inhibiting layering of one FGS onto another.[23] This folding maintains the high surface area of the FGSs when dry and helps to prevent layered aggregation between sheets when in suspension.

Recently graphene has generated considerable interest as an alternative to CNTs, since new manufacturing methods have indicated that graphene (in particular FGS) is much cheaper to produce at larger scales.[23,24] FGSs are also readily dispersible in many hydrocarbon fuels and propellants without the need of surfactants and may provide significantly higher surface area ($>$1800 m^2/g)[24] than their oxide counterparts, with heats of combustion close to that of aluminum (31.1 kJ/g of aluminum *versus* 32.8 kJ/g of carbon).[30] Moreover, because graphene is fully consumed by oxidation in high temperature processes containing an excess amount of oxygen, it can contribute to the fuel energy density, and its utilization will result in no exhaust particulate matter or plume "signature" beyond that of the fuel combustion products themselves.

The presence of nucleophilic oxygen-containing functionalities on the surfaces and edges of the FGSs imparts multifunctionality to the use of FGSs in fuels as these chemically active sites may provide catalytic behavior,[31] stabilizing or encouraging reaction intermediaries during combustion. Defect structures in the FGSs following reduction also provide active sites within the graphene structure. The high carrier mobility in graphene is little affected by low densities of defects,[23,29] which would serve to stabilize free radicals at the defect structure and so provide other sources of accessible nucleophiles within the FGS. The ability to set the C/O ratio of the FGS through chemical or thermal reduction permits tuning the FGS to specific solvents: the more reduced versions would be more compatible with alkanes while a higher oxygen content FGS (in the form of hydroxides, epoxides, and carboxylates) would be more compatible with more polar and/or ionic hydrocarbons such as the alcohols, aldehydes, and ketones.[23,24,27]

Here we wish to demonstrate the behavior of graphene colloidal suspensions on combustion properties and compare them with conventional metal oxide colloid behavior. We used nitromethane (CH_3NO_2 or NM), a highly energetic liquid organic nitro compound, in these demonstrations, because as a monopropellant the fuel and oxidizer are molecularly bound and any effects of fuel and oxidizer mixing rates on observations are minimized. Additionally, NM has long been identified as a potential rocket propellant for various applications and is receiving renewed interest as a low toxicity alternative to highly toxic propellants such as hydrazine.[32−37] As the simplest organic nitro compound, it also serves as a surrogate for more complex energetic materials, such as RDX (1,3,5-trinitrohexahydro-1,3,5-trizane, $(NO_2N \cdot CH_2)_3$), that share many of the same chemical reactions.[38] Due to NM's low oxygen content and reactivity, NM behaves as a fuel at low pressures, requiring additional oxidizers to sustain combustion. Therefore, NM is often referred to as both a fuel and a monopropellant.

Nitromethane, although a simple molecule, has a complex ignition and combustion process occurring in multiple stages.[38−40] The homogeneous reaction begins with the vaporization and decomposition of CH_3NO_2 through scission of the C−N bond, which is the initiating decomposition route and highly endothermic (activation barrier of 42 kcal/mol).[39] With the development of a pool of radical species, hydrogen abstraction from the methyl group of NM may also occur to yield CH_2NO_2. The first of two ignition stages is characterized by the consumption of NM and a rapid increase in temperature to an intermediate value, dependent on the initial temperature of the NM and environmental pressure. The rate of NM decomposition and the first stage ignition process are controlled by the NM dissociation reaction (i.e., $CH_3NO_2 + M \rightarrow CH_3 + NO_2 + M$). This stage is also characterized by the overall conversion of NO_2 to NO, yielding a considerable amount of CH_4 (via hydrogen abstraction by the methyl radical) and NO as the primary intermediate species, whose respective oxidation and reduction processes are relatively slow.[40] This creates an intermediate stage or "dark" zone, which can often be characterized by a plateau in the reaction temperature. The intermediate stage concludes with the onset of the second stage ignition process, which is characterized by a second rapid increase in temperature (to the equilibrium state), the overall reduction of NO to N_2, and the formation of product species such as CO, H_2O, H_2, and CO_2. Each ignition stage in the reaction process becomes progressively more exothermic.[40]
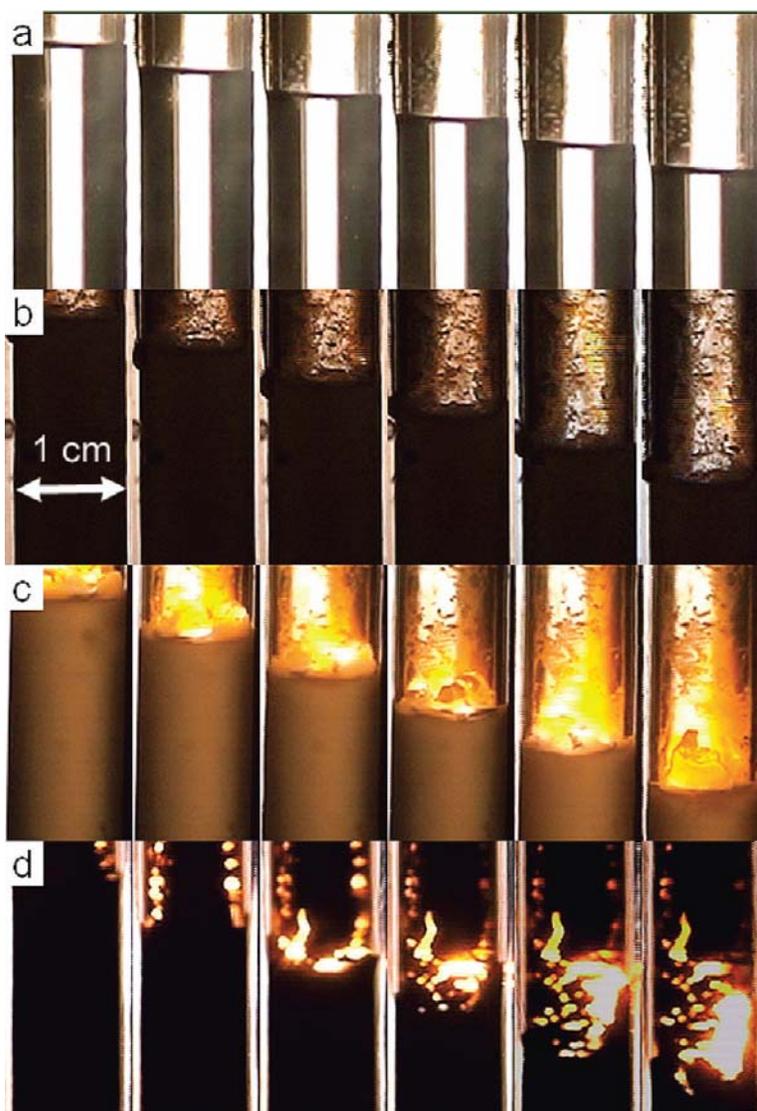

Figure 2. Captured images of regression process during combustion at 2 s intervals. (a) Neat nitromethane at 5.23 MPa, r_b = 1.2 mm/s. (b) NM containing 0.5 wt % Aluminum Oxide Plus at 5.16 MPa, r_b = 1.6 mm/s. (c) NM containing 0.39 wt % porous SiO_2 nanoparticles at 5.25 MPa, r_b = 1.9 mm/s. (d) NM containing 0.3% by mass FGS_{22} at 5.16 MPa, r_b = 2.2 mm/s. The fastest burn rate is achieved under roughly equivalent pressure through the addition of the smallest additive mass when using FGS_{22}. The residue left on the silica glass tube walls is much more apparent with FGS than the oxide materials, obscuring the view of much of the burning process; however under fuel lean conditions much of the FGS would be consumed though oxidation processes.

In what follows, we demonstrate that dispersing FGSs within NM can significantly enhance ignition and combustion rates without adding a catalytic compound to the graphene surface. A comparative analysis with oxide materials illustrates that, although burning rates are also increased by the addition of oxide nanoparticles, there are advantages to using the FGS rather than oxide nanoparticles. In this paper, we do not include a comparison with CNTs in nitromethane because of concerns about metal contamination in the CNTs. Metal contamination might affect the apparent combustion catalysis attributed to CNTs themselves. Catalytic activity of FGS is expected to occur on both sides of the
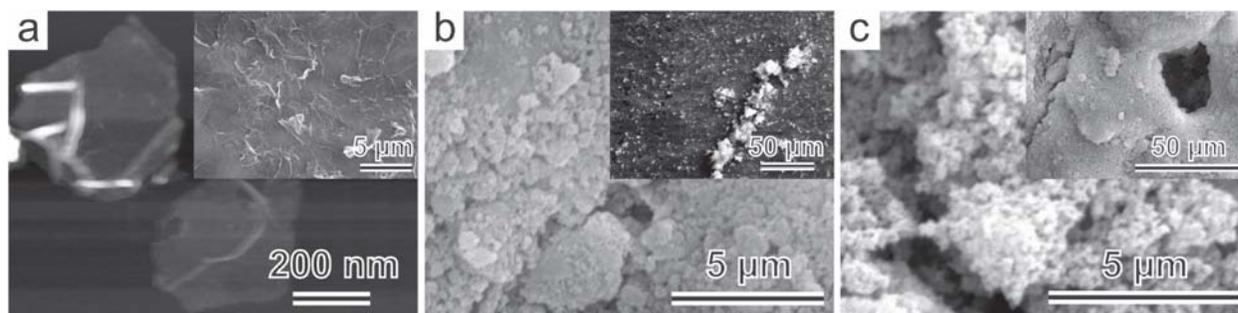
Figure 3. (a) AFM image of single sheet graphene (C/O ≈ 22). The inset is an SEM image of graphene agglomerates. Also shown are SEM images of (b) Nanoactive Aluminum Oxide Plus and (c) nanoporous silica.

graphene sheets. In the case of CNTs, however, the active surface is constrained to only the outer regions of the nanotubes. The fuel colloids studied, particularly ones containing FGSs, enhance the reaction rates through several mechanisms including enhanced heat transfer (radiation and conduction) and chemical reactivity (catalysis and carbon oxidation), a result we believe can be replicated in liquid fuels/air combustion problems involving petroleum derived and synthetic hydrocarbons. Several of these mechanisms are not yet fully understood, particularly those relating to the catalytic activity and heat transfer properties of the nanostructured materials. Future studies will lead to more fundamental investigations of these aspects and their relation to colloidal suspensions in fuel combustion.

RESULTS AND DISCUSSION

Various nanostructured fuel additives have been characterized and their effects on propellant energy density analyzed. Additionally, the linear deflagration (burning) rates (r_b, cm·s^{-1}) of nitromethane containing the colloidal additives were monitored and recorded (see Figure 2), characterizing the associated ignition and reaction rates as a function of additive concentration and system pressure. The linear burning rates are described using the commonly empirical relationship, $r_b = ap^n$, where n is known as the pressure exponent, and a is an empirical constant that is influenced by the initial propellant temperature.[41] The power law dependence on pressure is qualitatively supported by simple premixed flame theory.[42]

Characterization of Nanostructured Fuel Additives. Typical morphologies and overall dimensions of the silicon and aluminum oxides and FGS materials are shown in the scanning electron microscopy (SEM) images contained in Figure 3. Physical properties of the particles including the density and surface area are shown in Table 1. X-ray diffraction (XRD) analysis of the aluminum oxide (designated as Aluminum Oxide Plus by the supplier) demonstrates that it is aluminum monohydroxide (AlOOH), not aluminum oxide (Al$_2$O$_3$). XRD on the silicon oxide indicates an amorphous solid, having no detectable crystallinity. The FGS$_{22}$ powder did not exhibit any graphite-related diffraction peaks under XRD. Ther-

mal analysis of the respective powders indicated a high hydroxide content in the metal oxide powders, consistent with the assumed oxyhydroxide composition of the two metal oxides. FGS$_{22}$, being a highly reduced form of graphene oxide reacted in air near 800 °C.

The high surface areas of the three additives correspond to effective spherical radii of 2–3 nm for discrete primary particles of the densities shown in Table 1. As seen in Figure 3, agglomerates of the aluminum and silicon oxyhydroxide particles are much larger (micrometers to tens of micrometers) than this theoretical range, indicating the formation of "hard" agglomerates,[43] that is, agglomerates of primary particles that cannot be broken by the application of ultrasonic vibration.[44] These larger secondary particles have high porosity and may disperse readily in liquid under ultrasonic vibration. However, the larger particles quickly settle out of the liquid when agitation ceases. In contrast, the high surface area of the FGS reflects the high single sheet content of this material, which is also confirmed by atomic force microscopy studies.[23,24] High single sheet content, as well as its highly covalent structure lead the FGS sample to readily disperse in nitromethane. The resulting suspensions are far more stable than those of the metal oxyhydroxides, as is evidenced by little settling of the FGS of the liquid dispersion when agitation was removed.

Energetics of Nitromethane Mixtures. The combustion energetics of neat NM and the associated colloids were calculated using the NASA Chemical Equilibrium with Applications (CEA) Software.[45] Since the exact thermodynamic properties of the three additives used in this work are not available, they were modeled as pure SiO$_2$

TABLE 1. Physical Characterization of Nitromethane Additives

material	density, g/cm^3	surface area, m^2/g
functionalized graphene sheets (C/O = 22)	2.09–2.25	549
porous silica (5–15 nm)	2.2–2.6^a	590–690^a
	2.0 ± 0.1	514
NanoActive Aluminum Oxide Plus	2.9^a	>550^a
	2.7 ± 0.1	467

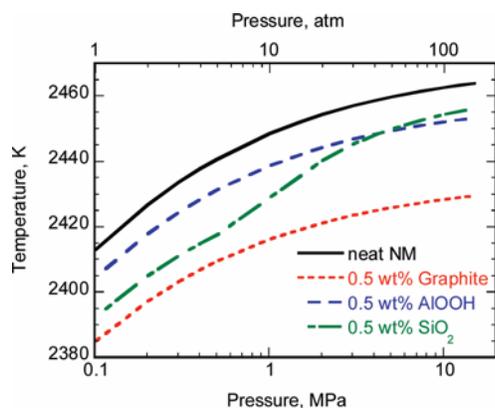^{a}Value provided by manufacturer or supplier.

Figure 4. Estimated equilibrium flame temperatures as a function of pressure for the propellants considered in this study. Calculations were completed using NASA CEA software, using an initial temperature of 298 K and a fuel additive concentration of 0.5% (by mass) which is on the order of the mixtures considered in the burning rate measurements. The thermochemistry of the colloid containing NanoScale Corporation's Aluminum Oxide Plus particles were modeled assuming a chemical makeup of $Al_2O_3(\alpha)$ and $Al(OH)_3(\alpha)$ as well, yielding only small differences (1−3 K) in the predicted flame temperatures when using boehmite. Assuming the enthalpy of formation of graphene to be equivalent to a C_{70} fullerene causes the predicted flame temperatures to be 6−8 degrees higher than when assumed equal to graphite. The shift in the silica curve is attributed to the transfer of reaction products from SiO to SiO_2 (l) at higher pressures.

(α-quartz), boehmite (AlOOH), and graphite since the thermodynamic properties of these materials are known. Figure 4 illustrates the calculated flame temperatures of each propellant as a function of pressure. NM is a monopropellant, that is, both the fuel and oxidizer properties are contained within the same molecular structure. Since NM has a negative oxygen balance (−39.3%),[46] the molecule is deficient in sufficient oxygen for complete combustion and all three additives reduced the reaction energetics by diluting the mixture. At these concentrations, the changes in the reaction energetics are small, indicating that burning rates should be slightly reduced by each of the additives present since flame temperatures are reduced, slowing reaction kinetics. Graphite reduces the flame temperatures the greatest amount but has the lowest density and molecular weight. Therefore, its volumetric and molar concentration would be the greatest. At lower pressures, alumina has the smallest effect, whereas at higher pressures the effects of silica and alumina are approximately the same. Fuel additives were also modeled using other materials of similar elemental composition and known thermochemistry, and only slight differences in the predicted temperatures were found.

Enthalpies of combustion were also calculated after adding a stoichiometric amount of oxygen. With oxygen present, the overall energetics were slightly affected by the low concentrations of additives considered; 0.5 wt % graphite increases the heat of reaction by 1.4%, while an equivalent amount of the silica and
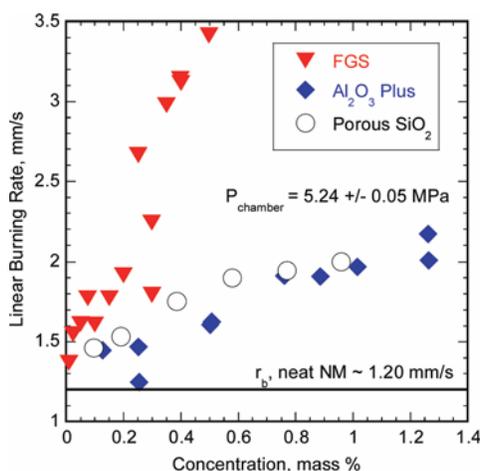

Figure 5. Linear burning rate of nitromethane and catalyst support additive mixtures as a function of mass concentration. The burning rate of neat NM is estimated using the experimentally derived correlation from Boyer and Kuo.[34]

boehmite decreased the heats of reaction by 0.65% and 0.003%, respectively.

Burning Rates of Nitromethane and Particle Dispersions. The burning rates of each mixture as a function of additive concentration are shown in Figure 5 (% mass) and Figure 6 (% volume). The results are compared with the neat NM burning rates derived by Boyer and Kuo, who used a similar experimental setup.[34] Each additive produced a significant enhancement in burning rates, implying that ignition delays were reduced and combustion rates were enhanced. Over the range of concentrations considered, increases in burning rates were roughly linearly proportional to the additive concentration. The two oxide materials had approximately the same effect, with the silica performing slightly better from a mass perspective. The NM burning rates were improved by nearly 60% with an oxide mass concentration of just 0.76 wt %. Although the results of the oxide colloids are noteworthy, the FGSs performed far better. A 47% gain in linear burning rate was found at a concentration as low as 0.075 wt %, with a maximum gain of greater than 175% using the FGS. When the results are viewed as a function of volume concentration there are only small differences in the trends, with FGSs still producing more significantly enhanced burning rates compared to the oxide additives. The FGS was not tested at concentrations greater than 0.5 wt % because some of the material coated the silica glass tube walls during testing, obstructing the view of the receding liquid column. Wall coating caused difficulty in resolving the flame images shown in Figure 2d.

Summarizing the observations above, the FGS suspension is superior to suspensions of the metal oxyhydroxides in two ways: First, FGS readily disperses into NM with the application of ultrasonic vibration and, second, more FGS remains in suspension for a longer time when the agitation is removed. The metal oxyhydroxides and the FGS had similar surface areas but quite dif-
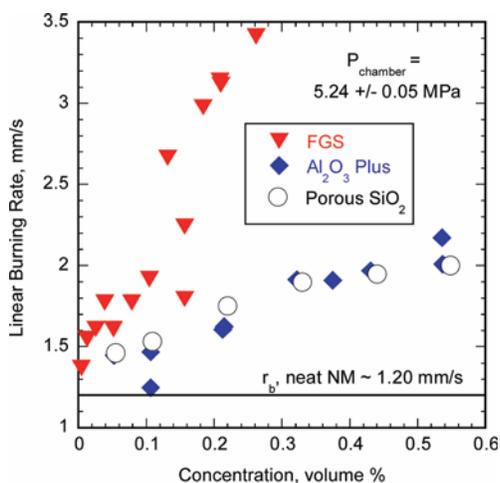
Figure 6. Linear burning rate of nitromethane and catalyst support additive mixtures as a function of volume concentration (density of FGS assumed to be 2.17 g/cm³). The burning rate of neat NM is estimated using the experimentally derived correlation from Boyer and Kuo.[34]
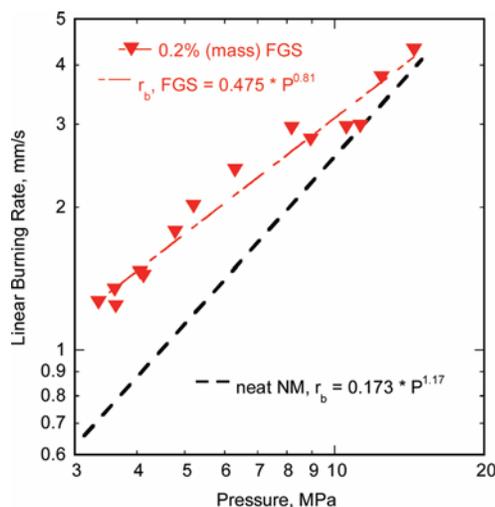

Figure 7. Linear burning rate of nitromethane and FGS additive mixtures as a function of pressure. The burning rate of neat NM is estimated using the experimentally derived correlation from Boyer and Kuo.[34] Burning rate correlations derived for the nitromethane mixtures using a curve fit to the data indicates a greatly reduced pressure exponent (*i.e.,* sensitivity).

ferent morphologies. Where the oxyhydroxides were limited by the presence of larger secondary particles, the FGS appears to contain a high fraction of single sheets (not visible in the SEM images but detailed in previous publications)[23,24] and planar aggregates with a high aspect ratio, as seen in Figure 3. Surface functionalities may be more accessible in this morphology, especially in comparison to functional groups held within the pores of porous secondary particles. The wetting of the additive by the NM is important here, as the penetration of the pores by the NM may be restricted by the oxide surfaces. In contrast, the oxygen-containing functional groups on FGS are contained on a highly covalent surface, enabling the FGS to act as an amphiphilic compound, having hydrophilic functional

groups on a hydrophobic substrate. Tuning the oxygen content through reduction of the FGS is possible and controlled reduction presents a mechanism by which the dispersibility of FGS in NM can be improved.

The effects of FGSs on the pressure dependence of the NM burning rate were determined, illustrated in Figure 7. Enhancements in burning rates due to FGS addition are greater under lower pressure conditions. At the highest pressures considered in this study, neat NM burning times are essentially equivalent to those of the colloid with 0.2 wt % FGSs. The colloid caused the NM burning process to display less pressure sensitivity over the range of pressures considered, which is important for propulsion applications such as rocket motors, where pressure instabilities lead to reduced motor control and performance. Since the reactor used in this study is limited to pressures below approximately 15 MPa, greater pressures could not be studied. As discussed hereafter, we expect that the colloid burning rates would follow the pressure dependency of neat NM at pressures greater than 15 MPa. Results of this study have also indicated that the pressure exponent is inversely proportional to the additive concentration, particularly at low concentrations.

Nitromethane Burning Rate Enhancement Mechanisms. The steady state linear deflagration rate of a liquid is controlled by the amount of heat released from the reaction, the reaction rate, and the rate of heat transfer from the gas-phase reaction back to the unreacted fluid. On the basis of the thermochemical calculations presented in Figure 4, it is known that the additives have a negligible or negative effect on the total heat release. Therefore increases in burning rates may be attributed to increased reaction rates and/or increased heat transfer. Heat transfer occurs *via* two modes, conduction and radiation. Solid bodies are known to absorb/emit a wide range of thermal radiation,[47] and nanoscale particles are known to have improved optical properties compared to large scale bulk materials.[7] The presence of particles within the liquid and entrained within the gas-phase reaction zone provides both emitters and receptors of thermal energy that are not present in the neat NM burning process. Carbon materials have high emissivities,[48] and therefore radiative heat transfer is expected to be greater with FGS additives. Radiative effects may be assumed to be independent of pressure, which provides an explanation for the pressure dependence of the observed burning rates. Given the reactivity of the FGSs it is unlikely that radiative heat transfer is the only burning rate enhancement mechanism. The thermal conductivity of single sheet graphene is quite large, at least equaling that measured for carbon nanotubes (∼4840 to 5300 W/m·K for graphene *versus* 1750−5800 W/m·K for single wall carbon nanotubes).[49] The heat sink capacity for the FGS-containing suspension is expected to be much higher than that of the NM alone or metal oxyhydroxide-containing suspensions.

The combustion of NM may be enhanced by catalyzing decomposition through eliminating the need to rupture the C−N bond.[50] The observed large enhancement in burning rates implies that the NM decomposition and subsequent reaction kinetics are accelerated by the presence of the high melting point particles. However, there is limited information involving the catalytic properties of metal oxides, oxyhydroxides, or carbon-based materials on NM. Hermoni and Salmon showed that a wide range of metal oxides could catalyze the first stage ignition and decomposition of NM.[51] "N-type" oxides produced the largest decrease in ignition temperatures, with alumina found to lower the ignition temperature to 260 °C, compared to the ignition temperature of neat NM at 419 °C.[52] Using these data, Benziger studied decomposition reactions using Ni, NiO, NiO/Al$_2$O$_3$ and Cr$_2$O$_3$/Al$_2$O$_3$ catalysts, concluding that NM adsorbs on the surface *via* the N−O oxygens and thereupon dissociates into absorbed HCN, O, and H. The rate limiting step is the breaking of the N−O bonds, which then desorb to form gaseous HCN, NH$_3$, N$_2$, and CO$_2$ products.[50,53] Unlike homogeneous decomposition, negligible amounts of NO$_x$ and CH$_4$ products were found. More recently, Yamaguchi demonstrated another mechanism for NM decomposition on a γ-alumina surface, showing the formation of aci-anions (CH$_2$NO$_2^-$),[54] a compound which has been identified as a sensitizing species in the detonation of liquid nitromethane.[55] The aci-anion then decomposed further into NCO, eventually forming NH$_3$ and CO$_2$ products.

Several mechanisms involving the functionalities on FGS are possible. Similar to the oxygen-containing functionalities in the metal oxyhydroxides, FGS functional groups are highly nucleophilic and accessible. Scission of the C−N bond through nucleophilic substitution reactions is one such mechanism, although adsorption onto the surface followed by decomposition of the N−O bond is another. We can only offer speculation at this time on possible catalytic mechanisms, but note that the improved dispersion of the FGS in the NM over that of the metal oxyhydroxides implies that more functional groups are in contact with the liquid for a given mass concentration of FGS with respect to the metal oxyhydroxides. Also, the reduced FGS is known to contain significant topographical defect structures. These defects can act as the sites for free radical formation and stabilization, offering mechanisms not present in the oxyhydroxides. But whatever the mechanism, the "dark" zone chemistry of the gas-phase reaction is in essence eliminated by these catalyzed decomposition reactions and the exothermicity of the initial stage of reaction is thereby increased. Homogeneous reactions, which are often second order, generally have rates proportional to the square of the pressure, whereas heterogeneous reaction rates usually increase linearly with pressure. Therefore, the catalytic effects of the particles will diminish with increasing pressure until their effects are negligible.

In addition to the catalytic routes for enhanced NM combustion, the oxides of nitrogen (NO, NO$_2$) are known to react with carbonaceous materials.[56−58] NO$_2$ reacts very rapidly with carbon at near 100 °C, and strong oxidative gasification of carbon occurs at temperatures greater than 400 °C.[57] Although carbon catalyzes the NO$_2$ decomposition reaction, it is unlikely to affect NM combustion processes since the homogeneous reaction is fast and modeling has not shown any significant concentrations of NO$_2$ occurring in the NM flame. The exothermic reactions between NO and carbon, which have similar kinetic rates as the O$_2$-carbon reactions, have been studied in detail due to their potential of controlling both soot and NO$_x$ engine emission levels. The NO reactions, which strongly gasify carbon above 600 °C,[57] are more likely to have an effect on NM burning rates. In nitromethane combustion, the NO is relatively unreactive at the "dark" zone temperature, and hence, large amounts of NO form and react slowly, until the second stage of reaction. By reacting NO with carbon, in the form of FGSs that are unbuffered by hydrogen, some of the energy release from the global reaction is shifted to lower temperatures and earlier times. Concentrations of NO are reduced as well, shortening the length of the "dark" zone at low pressures. These chemical mechanisms therefore lead to greater temperature gradients within the flame, increasing thermal conductivity from the flame to liquid−gas fuel interface. As a heterogeneous reaction, enhancements due to the carbon particle and NO reactions are reduced with pressure leading to the reduced pressure sensitivity found in Figure 7, as with catalytic mechanisms.

CONCLUSIONS

The linear burning rates of nitromethane have been studied at high pressures, exploring the effects of potential nanostructured catalyst support material additives, including aluminum oxyhydroxide, amorphous silicon oxide, and functionalized graphene sheets. In all cases burning rates were increased with the addition of these additives. Of the three materials considered, FGS proved to be the most promising in terms of maximizing the NM reaction rates. It is shown that the linear burning rate may be more than doubled with low concentrations of FGS. Burning rate enhancements were greatest at lower pressures, an attribute which caused the colloid burning rates to be less pressure sensitive than neat NM. Enhancement mechanisms are thought to be increased heat transfer due to radiation and thermal conductivity. Thermal conductivity is increased due to catalysis and the nitric oxide and FGS oxidation reaction, both of which reduce flame thicknesses at lower pressures. Further studies are required in order to determine the relative importance of each mechanism and fully understand the dynamics of FGS fuel colloid combustion. Although our current study presents results using only NM, we expect that a similar approach may be taken to improve the reaction rates of other liquid fuels such as hydrocarbons.

METHODS

Raw Materials. The nanostructured materials chosen for this study were porous silica (SiO_2) nanopowder (Sigma Aldrich, CAS No. 7631-86-9), Nanoactive Aluminum Oxide Plus (NanoScale Corp., Manhattan, KS), and FGSs with a C/O ratio of 22 (Princeton University, Princeton, NJ). The liquid monopropellant used was nitromethane (Alfa Aesar, CAS No. 75-52-5, 98+%). The fuel and additives were used as received.

FGS Synthesis Procedures. FGSs are synthesized through a thermal exfoliation process. This manufacturing process is described in detail in previous publications.[23,24] Graphite oxide (GO) is initially formed by oxidizing graphite flake (Asbury Carbons, Asbury, NJ) using a concentrated solution of nitric acid, sulfuric acid, and potassium chlorate following the Staudenmaier method.[59] At the completion of the oxidation process, GO is cleansed of the concentrated solution and spray dried. To exfoliate the GO, a small amount is placed into a silica glass tube that is sealed at one end, purged with argon, and placed into a high temperature furnace (Lindberg, model 59246-6, Lindberg/Blue M, Asheville, NC) for a set time period. High rates of CO_2 gas production yield pressures high enough to overcome the van der Waals forces holding the graphene layers together, prompting the exfoliation process. The conversion efficiency of this mechanism is therefore directly related to the furnace temperature used in the manufacturing process. A visual indication that FGSs have formed is a large volume expansion of the GO (500−1000 fold) which is verified by measuring the specific surface area of the products, elemental composition via X-ray photoelectron spectroscopy (XPS), and the disappearance of XRD peaks.

Particle Characterization. Density and surface areas of the solid additives were determined using a helium pycnometer (Accu-Pyc 1340, Micromeritics Instrument Corporation, Norcross, GA) and BET adsorption method (Gemini 2380, Micromeritics Instrument Corporation, Norcross, GA). The density of the FGS could not be accurately measured so the theoretical density of pristine graphite was used in Table 1.

The metal oxyhydroxide powders and FGS were characterized by scanning electron microscopy (5130MM, Tescan, Czech Republic) to determine particle size and microscopic features. SEM samples of the colloids were prepared by first ultrasonicating each powder in ethanol, then putting a drop onto a conductive aluminum sample stub and allowing the solvent to evaporate. The metal oxyhydroxide samples were coated with 2−3 nm of iridium to ensure good conductivity and imaging. FGS samples were sufficiently conductive and did not require metal coating.

X-ray diffraction analysis was performed on dry powder samples to determine the phase content and the extent of crystallinity in the respective colloids (Miniflex diffractometer, Cu Kα radiation, $\lambda = 1.5406$ Å, Rigaku Americas Corp., The Woodlands, TX). Simultaneous thermal gravimetric analysis (TGA) and differential scanning calorimetry (DSC) were done to corroborate XRD analysis of the colloids (STA 449C Jupiter, Erich Netzsch GmbH & Co., Germany). Samples were ramped to 1100 °C under air at 20 °C, sufficient to completely combust the FGS and chart phase transitions in the aluminum oxyhydroxide powder.

Thermochemical Calculations. Equilibrium flame temperatures of neat nitromethane and colloids were estimated using Chemical Equilibrium with Applications (CEA) software (National Aeronautics and Space Administration, Lewis Research Center, Cleveland, OH).[45] The "combustion" problem type was used, which assigns a constant pressure and enthalpy for the reaction. Standard enthalpies of formation for NM, graphite, silica, alumina, and aluminum hydroxide ($Al(OH)_3$) materials were provided in the CEA thermochemistry databases. Enthalpies of C_{70} fullerene and boehmite were applied from other sources.[60,61] Heats of combustion (i.e., enthalpies of reaction) were calculated assuming a reaction temperature and pressure of 298 K and 1 atm, and the only reaction products to be CO_2, H_2O (l), N_2, Al_2O_3, and SiO_2, depending on the monopropellant considered. Enthalpies of formation for all materials with the exception of boehmite were taken from the National Institute of Standards and Technology (Gaithersburg, MD) database.[62]

Liquid Dispersion Preparation. Constituents of each mixture were measured on a mass basis using an analytical balance (model AB265-S, Mettler Toledo, Columbus, OH) into a tall screw top vial (23.5 mL (6 drams)). The particles were initially mixed by shaking the vial by hand and were then dispersed using an ultrasonic bath (model 150, VWR, West Chester, PA) for a minimum of 45 min to reduce particle agglomeration. All samples were dispersed immediately prior to burning rate testing to minimize any effects related to particle agglomeration and sedimentation.

Burning Rate Measurement Procedures. The effect of the NM additives on the combustion rates was determined by measuring the linear burning rate of the colloids in a large (23 L) constant volume optical pressure vessel or strand burner. Before loading the sample into the reactor, the suspension was transferred using a pipet from the vial to a silica glass tube (10 mm O.D. × 8 mm I.D.), which was a minimum of 5 cm long and capped at one end. The samples are placed into silica glass tubes so that the burning process may be optically observed. Argon was used to pressurize the vessel, reducing the concentration of oxygen containing species to negligible quantities. The absence of oxygen in the system required that the vessel be pressurized to reduce the reaction zone thickness, and obtain a steady state, self-propagating combustion process of the NM. Real time recording of the reaction progression was monitored using a digital video camera recorder (Sony, model DCR-SR100). The chamber, experimental setup, and basic procedure is described in more detail and shown schematically in a previous publication.[63]

As a fuel-rich premixed fuel and oxidizer mixture (or monopropellant), there is no need to provide a separate oxidizer with the NM. Ignition of each sample was accomplished using an ignition booster made of double-base gun propellant (NOSOL 363), threaded over a strand of nichrome wire, which is placed slightly submerged at the top of the liquid column. The nichrome wire is resistively heated using a power supply (Agilent Technologies, model 6674A, Santa Clara, CA) with an applied load of 45 W (9 V, 5 A) to ignite the booster, which in turn ignites the NM. A Nicolet Genesis multichannel data acquisition system (LDS Nicolet, model 986A0151, Middleton, WI) monitored and recorded the system pressure (Setra, model 206 pressure transducer, 0−5000 psig, Boxborough, MA) as a function of time at a standard sampling rate of 200 Hz, while the receding liquid column was recorded using the video camera. Burning rates are determined from the digital video, which recorded the process at a rate of 30 frames per second. The outer diameter of the silica glass tube is used as the reference dimension.

REFERENCES AND NOTES

1. Edwards, T. Liquid Fuels and Propellants for Aerospace Propulsion: 1903−2003. *J. Propul. Power* **2003**, *19*, 1089–1107.
2. Maurice, L. Q.; Lander, H.; Edwards, T.; Harrison III, W. E. Advanced Aviation Fuels: A Look Ahead via a Historical Perspective. *Fuel* **2001**, *80*, 747–756.
3. Astbury, G. R. A Review of the Properties and Hazards of Some Alternative Fuels. *Process Saf. Environ.* **2008**, *86*, 397–414.
4. Ramadhas, A. S.; Jayaraj, S.; Muraleedharan, C. Use of Vegetable Oils as I.C. Engine Fuels—A Review. *Renew. Energy* **2004**, *29*, 727–742.
5. Wickham, D. T.; Cook, R. L.; De Voss, S.; Engel, J. R.; Nabity, J. Soluble Nanocatalysts for High Performance Fuels. *J. Russ. Laser Res.* **2006**, *27*, 552–561.
6. Wickham, D. T.; Cook, R. L.; Engel, J.; Jones, M.; Nabity, J. Soluble Nanocatalysts for High Performance Fuels.

Presented at the 19th ONR Propulsion Meeting, Los Angeles, CA, December 20, 2006.

7. Ichinose, N., Ozaki, Y. Kashu. S. *Superfine Particle Technology*; Springer-Verlag: New York, 1992.

8. Chehroudi, B.; Vaghjiani, G. L.; Ketsdever, A. D. Method for Distributed Ignition of Fuels by Light Sources. U.S. Patent 7,517,215 B1, April 14, 2009.

9. Choi, S. U. S. Enhancing Thermal Conductivity of Fluids with Nanoparticles. Presented at the ASME International Mechanical Engineering Congress and Exposition, San Francisco, CA, 1995; American Society of Mechanical Engineers: pp 99−105.

10. Das, S. K.; Choi, S. U. S.; Yu, W.; Pradeep, T. *Nanofluids: Science and Technology*; John Wiley & Sons: Hoboken, NJ, 2008.

11. Eastman, J. A.; Phillpot, S. R.; Choi, S. U. S.; Keblinski, P. Thermal Transport in Nanofluids. *Annu. Rev. Mater. Res.* **2004**, *34*, 219–246.

12. Yu, W.; France, D. M.; Routbort, J. L.; Choi, S. U. S. Review and Comparison of Nanofluid Thermal Conductivity and Heat Transfer Enhancements. *Heat Transfer Eng.* **2008**, *29*, 432–460.

13. Song, J.; Wang, J.; Boehman, A. L. The Role of Fuel-Borne Catalyst in Diesel Particulate Oxidation Behavior. *Combust. Flame* **2006**, *146*, 73–84.

14. Valentine, J. M.; Peter-Hoblyn, J. D.; Acres, G. K. Emissions Reduction and Improved Fuel Economy Performance From a Bimetallic Platinum/Cerium Diesel Fuel Additive at Ultra-Low Dose Rates. Presented at the CEC/SAE Spring Fuels & Lubricants Meeting & Exposition, Paris, France, June, 2000.

15. Amariei, D.; Courtheoux, L.; Rossignol, S.; Batonneau, Y.; Kappenstein, C.; Ford, M.; Pillet, N. Influence of Fuel on Thermal and Catalytic Decompositions of Ionic Liquid Monopropellants. Presented at the 41st AIAA/ASME/SAE/ASEE Joint Propulsion Conference and Exhibit, Tucson, AZ, July 10−13, 2005.

16. Mellor, B.; Ford, M. Investigation of Ignition Delay with DMAZ Fuel and MON Oxidiser. Presented at the 42nd AIAA/ASME/SAE/ASEE Joint Propulsion Conference and Exhibit, Sacramento, CA, July 9−12, 2006.

17. Mench, M. M.; Yeh, C. L.; Kuo, K. K. Propellant Burning Rate Enhancement and Thermal Behavior of Ultra-fine Aluminum Powders (Alex). Presented at the 29th International Annual Conference of ICT, Karlsruhe, Germany, June 30−July 3, 1998; pp 1−15.

18. Risha, G. A.; Boyer, E.; Wehrman, R. B.; Kuo, K. K. Performance Comparison of HTPB-Based Solid Fuels Containing Nano-Sized Energetic Powder in a Cylindrical Hybrid Rocket Motor. Presented at the 38th AIAA/ASME/SAE/ASEE Joint Propulsion Conference, Indianapolis, IN, July 7−10, 2002.

19. Risha, G. A.; Boyer, E.; Evans, B.; Kuo, K. K.; Malek, R. Characterization of Nano-Sized Particles for Propulsion Applications. *Mater. Res. Soc. Symp. Proc.* **2004**, *800*, AA6.6.1.

20. Risha, G. A.; Sabourin, J. L.; Son, S. F.; Tappan, B.; Yang, V.; Yetter, R. A. Combustion and Conversion Efficiency of Nanoaluminum-Water Mixtures. *Combust. Sci. Technol.* **2008**, *180*, 2127–2142.

21. Tyagi, H.; Phelan, P. E.; Prasher, R.; Peck, R.; Lee, T.; Pacheco, J. R.; Arentzen, P. Increased Hot-Plate Ignition Probability for Nanoparticle-Laden Diesel Fuel. *Nano Lett.* **2008**, *8*, 1410–1416.

22. Johnson, C. E.; Fallis, S.; Chafin, A. P.; Groshens, T. J.; Higa, K. T.; Ismail, I. M. K.; Hawkins, T. W. Characterization of Nanometer- to Micron-Sized Aluminum Powders: Size Distribution from Thermogravimetric Analysis. *J. Propul. Power* **2007**, *23*, 669–682.

23. Schniepp, H. C.; Li, J.; McAllister, M. J.; Sai, H.; Herrera-Alonso, M.; Adamson, D. H.; Prud'homme, R. K.; Car, R.; Saville, D. A.; Aksay, I. A. Functionalized Single Graphene Sheets Derived from Splitting Graphite Oxide. *J. Phys. Chem. B* **2006**, *110*, 8535–8539.

24. McAllister, M. J.; Li, J.; Adamson, D. H.; Schniepp, H. C.; Abdala, A. A.; Liu, J.; Herrera-Alonso, M.; Milius, D. L.; Car, R.; Prud'homme, R. K.; Aksay, I. A. Single Sheet Functionalized Graphene by Oxidation and Thermal Expansion of Graphite. *Chem. Mater.* **2007**, *19*, 4396–4404.

25. Geim, A. K.; Novoselov, K. S. The Rise of Graphene. *Nat. Mater.* **2007**, *6*, 183–191.

26. Ramanathan, T.; Abdala, A. A.; Stankovich, S.; Dikin, D. A.; Herrera-Alonso, M.; Piner, R. D.; Adamson, D. H.; Schniepp, H. C.; Chen, X.; Ruoff, R. S.; *et al*. Functionalized Graphene Sheets for Polymer Nanocomposites. *Nat. Nanotechnol.* **2008**, *3*, 327–331.

27. Stankovich, S.; Dikin, D. A.; Piner, R. D.; Kohlhaas, K. A.; Kleinhammes, A.; Jia, Y.; Wu, Y.; Nguyen, S. T.; Ruoff, R. S. Synthesis of Graphene-Based Nanosheets *via* Chemical Reduction of Exfoliated Graphite Oxide. *Carbon* **2007**, *45*, 1558–1565.

28. Lerf, A.; He, H.; Forster, M.; Klinowski, J. Structure of Graphite Oxide Revisited. *J. Phys. Chem. B* **1998**, *102*, 4477–4482.

29. Kudin, K. N.; Ozbas, B.; Schniepp, H. C.; Prud'homme, R. K.; Aksay, I. A.; Car, R. Raman Spectra of Graphite Oxide and Functionalized Graphene Sheets. *Nano Lett.* **2008**, *8*, 36–41.

30. Kuo, K. K.; Risha, G. A.; Evans, B.; Boyer, E. Potential Usage of Energetic Nano-sized Powders for Combustion and Rocket Propulsion. *Mater. Res. Soc. Symp. Proc.* **2004**, *800*, 3–14.

31. Fowler, J. D.; Allen, M. J.; Tung, V. C.; Yang, Y.; Kaner, R. B.; Weiller, B. H. Practical Chemical Sensors from Chemically Derived Graphene. *ACS Nano* **2009**, *3*, 301–306.

32. Zwicky, F.; Ross, C. C. Nitromethane Excels as Rocket Propellant. *Soc. Automot. Eng. J.* **1949**, *57*, 22–24.

33. Anon. Evaluate Nitromethane for Rockets. *Aviat. Week* **1949**, 27–33.

34. Boyer, E.; Kuo, K. K. High-Pressure Combustion Behavior of Nitromethane. Presented at the 35th AIAA/ASME/SAE/ASEE Joint Propulsion Conference, Los Angeles, CA, June 20−24, 1999.

35. Kelzenberg, S.; Eisenreich, N.; Eckl, W.; Weiser, V. Modelling Nitromethane Combustion. *Propellants, Explos., Pyrotech.* **1999**, *24*, 189–194.

36. Boyer, E.; Kuo, K. K. Modeling of Nitromethane Flame Structure and Burning Behavior. *Proc. Comb. Inst.* **2006**, *31*, 2045–2053.

37. Boyer, E.; Kuo, K. K. Characteristics of Nitromethane for Propulsion Applications. Presented at the 44th AIAA Aerospace Sciences Meeting and Exhibit, Reno, NV, January 9−12, 2006.

38. Boyer, E.; Kuo, K. K. Modeling of Nitromethane Flame Structure and Burning Behavior. *Proc. Combust. Inst.* **2007**, *31*, 2045–2053.

39. Guirguis, R.; Hsu, D.; Bogan, D.; Oran, E. A Mechanism for Ignition of High-Temperature Gaseous Nitromethane—The Key Role of the Nitro Group in Chemical Explosives. *Combust. Flame* **1985**, *61*, 51–62.

40. Melius, C. F. Thermochemistry and Reaction Mechanisms of Nitromethane Ignition. *J. Phys. IV* **1995**, *5*, 535–552.

41. Sutton, G. P. *Rocket Propulsion Elements: An Introduction to the Engineering of Rockets,* 6th ed.; John Wiley & Sons, Inc.: New York, 1992; pp 374−375.

42. Glassman, I. *Combustion,* 3rd. ed.; Academic Press: San Diego, 1996.

43. Lange, F. F.; Davis, B. I.; Aksay, I. A. Processing-Related Fracture Origins: III. Differential Sintering of ZrO_2 Agglomerates in Al_2O_3/ZrO_2 Composite. *J. Am. Ceram. Soc.* **1983**, *66*, 407–408.

44. Aksay, I. A.; Lange, F. F.; Davis, B. I. Uniformity of Al_2O_3-ZrO_2 Composites by Colloidal Filtration. *J. Am. Ceram. Soc.* **1983**, *66*, C190−C192.

45. McBride, B. J.; Gordon, S. *Computer Program for Calculation of Complex Chemical Equilibrium Compositions and Applications*; NASA: Washington, DC, 1996.

46. Kubota, N. *Propellants and Explosives*; Wiley-VCH: Weinheim, Germany, 2001.

47. Siegel, R. *Thermal Radiation Heat Transfer*; Taylor & Francis: London, 2002.

48. Touloukian, Y. S. *Thermal Radiative Properties—Nonmetallic Solids*; Thermophysical Properties of Matter, Vol 8; IFI/Plenum: New York, 1972.

49. Balandin, A. A.; Ghosh, S.; Bao, W. Z.; Calizo, I.; Teweldebrhan, D.; Miao, F.; Lau, C. N. Superior Thermal Conductivity of Single-layer Graphene. *Nano Lett.* **2008**, *8*, 902–907.

50. Benziger, J. *A Mechanistic Study of Nitromethane Decomposition on Ni Catalysts*; AFOSR-TR-83-0405; National Technical Information Service: Alexandria, VA, 1982; Paper No. ADA128444.

51. Hermoni, A.; Salmon, A. Effect of Various Oxides on the Decomposition Temperature of Nitroparaffins. *Chem. Ind.* **1960**, 1265.

52. Glassman, I.; Yetter, R. A. *Combustion*; Academic Press: Burlington, MA, 2008.

53. Benziger, J. Decomposition of Nitromethane over NiO and Cr_2O_3 Catalysts. *Combust. Sci. Technol.* **1982**, *29*, 191–205.

54. Yamaguchi, M. Decomposition of Adsorbed Nitromethane on γ-Alumina. *J. Chem. Soc., Faraday Trans.* **1997**, *93*, 3581–3586.

55. Engelke, R.; Earl, W. L.; Rohlfing, C. M. Microscopic Evidence That the Nitromethane Aci Ion Is a Rate Controlling Species in the Detonation of Liquid Nitromethane. *J. Chem. Phys.* **1986**, *84*, 142–146.

56. Aarna, I.; Suuberg, E. M. A Review of the Kinetics of the Nitric Oxide−Carbon Reaction. *Fuel* **1997**, *76*, 475–491.

57. Stanmore, B. R.; Tschamber, V.; Brilhac, J.-F. Oxidation of Carbon by NO_x, with Particular Reference to NO_2 and N_2O. *Fuel* **2008**, *87*, 131–146.

58. Tighe, C. J.; Dennis, J. S.; Hayhurst, A. N.; Twigg, M. V. The Reactions of NO with Diesel Soot, Fullerene, Carbon Nanotubes, and Activated Carbons Doped with Transition Metals. *Proc. Combust. Inst.* **2009**, *32*, 1989–1996.

59. Staudenmaier, L. Verfahren zur Darstellung der Graphitsäure. *Ber. Dtsch. Chem. Ges.* **1898**, *31*, 1481.

60. Cioslowski, J.; Rao, N.; Moncrieff, D. Standard Enthalpies of Formation of Fullerenes and Their Dependence on Structural Motifs. *J. Am. Chem. Soc.* **2000**, *122*, 8265–8270.

61. Knacke, O.; Kubaschewski, O.; Hesselmann, K., *Thermochemical Properties of Inorganic Substances,* 2nd ed.; Verlag Stahleisen: Dusseldorf, Germany, 1991.

62. Linstrom, P. J.; Mallard, W. G. NIST Chemistry WebBook, NIST Standard Reference Database Number 69. In National Institute of Standards and Technology: Gaithersburg, MD, 2009.

63. Risha, G. A.; Son, S. F.; Yetter, R. A.; Yang, V.; Tappan, B. C. Combustion of Nano-Aluminum and Liquid Water. *Proc. Combust. Inst.* **2007**, *31*, 2029–2036.